Optimizing the Effect of Solid Lubricants on the Sliding Wear Behavior of SiC$_p$ Reinforced Cast Aluminum Alloy

Mohammad Mohsin Khan[1] · Mohammad Irfan Hajam[1] · Zahoor Ahmad Mir[1]

Abstract

The present study's objective is to investigate the impact of adding solid lubricants (graphite, molybdenum disulfide, titanium dioxide) to SAE20-40 oil on the sliding wear performance of as-cast SiC dispersed aluminum alloy. Matrix alloy and conventionally used Gunmetal were also tested under identical conditions to understand the scope of latter material as a possible substitute in various engineering applications. The Taguchi's L$_{27}$ orthogonal array is considered for conducting experiments through three input parameters, i.e., Test Materials, Test Environment, and Applied Load. Based on the results, the analyses are carried out using analysis of variance. From the main effects plot, the optimum condition is obtained LM13S10 composite under MoS$_2$ lubrication at 50 N load.

Keywords Sliding wear · Light metal alloy · Composites · SEM · Solid lubricants · Optimization technique

1 Introduction

In the last few decades, many researchers' attention to Metal Matrix Composites (MMCs) has significantly increased due to the increase in demand for lightweight and rigid materials for the aerospace, aviation, and automotive industries. They are considered as potential engineering materials owing to having outstanding mechanical and tribological properties [1]. Among a diverse range of accessible matrix material, aluminum-based alloys have several benefits, including higher strength, low density, excellent thermal conductivity, and a lower friction coefficient [2]. Despite having mentioned properties, their weak wear resistance property restricts their use as promising material [3]. However, to enhance their mechanical and tribological properties, reinforcements, either hard or soft type, were added to the aluminum matrix to cope with stringent material requirements in different applications. In this regard, a variety of aluminum-based alloys such as AA2024 [4–7], AA3003 [8], AA4043 [9], AA5052 [10, 11], AA5083 [12], AA6061 [13–17], AA6082 [18], AA6360 [19], AA7075 [20, 21], A356 [2, 22, 23], A383 [3, 24], LM4 [25], LM6 [26], and

LM13 [27] have been used as the matrix alloy. Various kinds of reinforcements such as SiC [2, 15, 16, 21, 24, 27–32], B$_4$C [17, 19, 22, 23], TiC [10, 19, 33], WC [34], Al$_2$O$_3$ [7, 15, 35–38], TiO$_2$ [8], ZrO$_2$ [39, 40], TiB$_2$ [41], ZrB$_2$ [11], CNT [42], Graphene [13], Red Mud [18, 43], Graphite [44] have been commonly used with an objective to realize property improvement of the alloy system. However, silicon carbide (SiC) is the most commonly employed reinforcement particulates for AMCs than other reinforcing materials [45].

The SiC being slightly denser than that of Aluminum alloy offered a challenge. SiC's chemical compatibility and adequate bonding with the matrix material tackled the said challenge without developing an intermetallic phase. Compared to other reinforcement materials, low-cost, good thermal conductivity and workability make it a good alternative [15]. Kumar et al. [16] studied the influence of SiC on an Al6061–SiC composite's hardness. They found that the relative increase in hardness up to 67% with 6 wt.% SiC reinforcement was achieved. This improvement can be attributed to the higher hardness of SiC. The presence of SiC in the composite provides an improvement in its hardness.

In the literature, a variety of processing methods for the synthesis of AMCs are available, such as stir casting [17], squeeze casting [6], rheocasting [46], spray deposition [29], powder metallurgy [37], and mechanical alloying [47]. Besides the type of application, the selection of synthesis process primarily depends on the reinforcement's shape,

✉ Mohammad Mohsin Khan
  mohsinkhan@nitsri.ac.in

1   National Institute of Technology Srinagar, Srinagar, India

size, and volume fraction. The alloy is then prepared by melting the Al matrix completely, followed by the careful addition of SiC ceramic [24, 30] with a mechanical stirrer [7].

Several studies have been reported on the sliding wear behavior of different ceramic particle-reinforced aluminum composites. They indicate that the wear behavior is elaborate, dependent on the synergistic effects of operational and material-related conditions [48]. Also, Experimental factors (such as velocity, distance, conditions, load) control the wear behavior.

Mixed lubrication condition involving metal-to-metal contact in part is experienced in sliding applications in the events of delayed lubrication and starting and stopping operations [49, 50].

In such applications, liquid and semi-solid lubricants are used [51]. Additives help to improve lubricant performance [5, 49–52]. It is important to note that solid lubricants in the mixture of liquid/semi-solid lubricants are beneficial to vary degrees depending on the nature and content of the matrix of additives and lubricants [52].

Solid lubricant particles' role in controlling wear behavior when present within the material system depends on pressure, sliding speed, environment, the shape and size of the lubricant particles, and the nature of interfacial bonding between particles/matrix.

Studies have revealed that specific material under specific test conditions yield positive effects in solid lubricants [53, 54]. For example, by generating appropriate microstructural features such as spherical micro constituents and sound particle/matrix interfacial bonding in the material, a solid lubricant's advantages can be realized so that the lubricant film formation becomes effective [53, 54]. Another way to understand the advantages of solid lubricants could be by adding them to a base lubricant such as oil/grease [49–52]. Solid lubricant particles added externally together with a base (oil) lubricant on the sliding surfaces produce better results [52] as the particles enjoy a more efficient interaction with the contacting surfaces and a greater ability to smear and adhere to them, thus creating more stable films/layers of lubrication and improving wear response [52, 54]. This practice also nullifies the possible adverse effects of material parameters such as dispersoid/matrix interfacial features and the nature, morphology, and mode of distribution of different microconstituents.

Available solid lubricants are mostly lamellar solids [55], which allow them to easily smear along the contacting surfaces producing a lubricating effect and improving wear performance. Molybdenum disulfide (MoS_2) is a fine example of solids that are stacked. Fullerene systems can accommodate huge loads and speeds. However, they often oxidize and become inactive above 450 °C. Graphite is a very well-known solid lubricant used in all commercial lubrication applications with lamellar structure. For good lubricity, it needs moisture. Graphite blends and pure graphite dry film are commonly used for applications such as hot and cold shaping, wire drawing and billet grinding, high-speed cutting tools, as a mold release for die casting operations, plastic and rubber molding applications, cylinder head and exhaust bolts, weapons and armament applications, automobile engines and many other industrial applications. Titanium dioxide is an environmentally friendly lubricant that, like other solid lubricants described above, does not have lamellar morphology [56].

Based on the literature survey, the effects of SiC reinforcement appear to have been observed to a limited extent on the lubricated sliding wear behavior of an aluminum alloy system. In contrast, the optimization of sliding wear characteristics under solid lubricants' influence is not fully explored. Therefore, an attempt was made in this analysis to examine the sliding wear behavior of an aluminum alloy and its composite reinforced with 10 wt. % of SiC particles under the influence of solid lubricants (MoS_2, Graphite, and TiO_2). Further, the wear characteristics of SiC reinforced composite have been compared with conventionally used Gunmetal. A correlation has been established between wear, friction, and temperature with the applied load by selecting the performance characteristics using an L27 array orthogonal design.

2 Taguchi Method

The Taguchi method, a statistical method developed by G. Taguchi, is a measure of robustness used to identify variability in a process/product to determine the best control parameters and minimize noise factors(uncontrollable factors) [57]. The S/N ratio measures how the target/nominal value response varies under different noise conditions. Depending on the experiment's goal, there are three S/N ratios; Larger is better, Nominal is best, Smaller is better. The procedure can be summarized as

- Identify and evaluate quality characteristics and process parameters
- Identify the objective function
- Identify the number of levels and possible interactions for the process parameters
- Select an appropriate standard orthogonal array (OA)
- Conduct experiments based on the run order of the orthogonal array
- Analyze data using S/N ratio and ANOVA and predict the optimum conditions
- Perform a verification experiment.

3 Materials and Methods

3.1 Material Selection

In the work presented, LM13 has been chosen as the matrix material for preparing the metal matrix composite. The advantage of good resistance to wear, good bearing properties, and a low thermal expansion coefficient makes it suitable to be used for pulley sheaves, pistons for all types of diesel and petrol engines, and other engine parts operating at higher temperatures. Furthermore, SiC has been selected as a reinforcing material, which is very hard compared to aluminum alloy. The density of the matrix and reinforcement is approximately the same. The advantages over other reinforcement materials include its high thermal conductivity, good tensile and flexural strength, excellent resistance to erosion, corrosion, and chemical attacks in reducing environments [31].

3.2 Synthesis of the Test Materials

The test materials (alloy and composite) were synthesized by melting and casting techniques. Melting was performed using an electric furnace in graphite crucibles. A mechanical stirrer was used to create the molten alloy vortex, in which 10 wt. % of the preheated SiC particles (particle size ~ 50–100 μm) were dispersed. The melts were solidified in 14 mm diameter, 170 mm long cylindrical casting in preheated cast-iron molds. The melting process's schematic is shown in Fig. 1, whereas Table 1 shows the casted materials' chemical compositions.

3.3 Microstructural Observation

Scanning Electron Microscope (JSM-7100F JEOL, Germany) was used for Microstructural observations. The test specimens were polished using conventional metallographic methods, including polishing the sample with various grades of emery papers and eventually using a polishing cloth with fine alumina paste. After polishing, aluminum samples were etched using Keller's reagent and (10 g $FeCl_3$ + 50 ml HCl + 200 ml distilled water) was used for Gunmetal to observe grain structures and metal matrix interfaces.

3.4 Hardness Measurement

The hardness of the test materials has been evaluated with the Vickers' hardness tester. The samples were polished and appropriately cleaned before measurement. The load of 30 kg was applied to all the samples when measuring hardness. An average of five readings has been reported in this study.
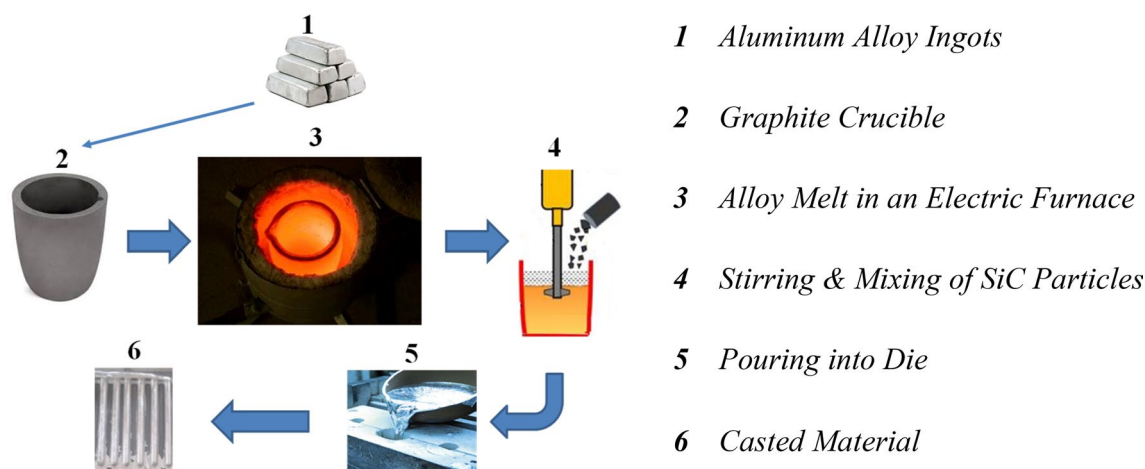

1 Aluminum Alloy Ingots

2 Graphite Crucible

3 Alloy Melt in an Electric Furnace

4 Stirring & Mixing of SiC Particles

5 Pouring into Die

6 Casted Material

Fig. 1 A schematic representation of the composite preparation

Table 1 Elemental weight composition of the cast material

Material	Element wt. percentage									
	Si	Fe	Cu	Mn	Mg	Ni	Cr	Zn	SiC	Al
LM13	11.8	0.25	0.6	0.15	1.7	1.5	0.1	0.25	–	Balance
LM13S10	11.8	0.25	0.6	0.15	1.7	1.5	0.1	0.25	10	Balance

Gunmetal is procured from external sources

3.5 Sliding Wear Tests

Ducom (India) made pin-on-disk machine was used to perform sliding wear tests as per ASTM G99-05 standard [58]. Figure 2 shows the schematic representation of wear test analysis. Cylindrical test pins (10 mm diameter and 30 mm length) were held against a rotating EN31 steel disk (1.02% C, 1.05% Cr, 0.3% Ni, 0.35% Mn and remainder Fe). The steel disk was mechanically polished to a roughness (Ra) level of 1–2 μm before each test. 5 wt. % of commercially available solid lubricants (graphite, molybdenum disulfide, titanium dioxide) with an average particle size of 7–10 μm were mixed in SAE 20W-40 oil to create the lubricating condition. Sliding wear tests were conducted at a sliding speed of 2.1 m/s over an applied load range of 50, 100 and 150 N. The test method involved inserting and permitting the disk to rotate in a lubricant mixture for 5 s at a speed of 3.35 m/s. The lubricated disk has been rotated so that the surplus lubricant is spun off, and uniform thickness of lubricant is obtained. Thus, the conditions were maintained similar to mixed lubrication. The sample was fixed in the specimen holder, enabling the disk to rotate at the specified sliding speed up to a specified distance of 2500 m or until the specimen seizer. Frictional heating was measured using a chromel–alumel thermocouple implanted into a 1.5 mm diameter hole on the 1.5 mm sample pin from the sliding surface.

The thermocouple output is fed to a computer-based information logging system where the sample's friction heating is continually recorded during each experiment. The loads were vertically applied to the pin sample against the disk. The strain gauge result is also transferred to a computer-based data logging system that records every experiment's tangential load on the sample pin. The friction coefficient has been calculated by dividing the tangential load with the applied normal load. The specimens had been thoroughly cleaned and measured before and after each test.

A Denver make microbalance has been used to weigh the samples. Weight loss was then transformed into volume loss per unit sliding distance for wear rate measurement.

3.6 Design of Experiment

Design of experiment (DOE) is a methodology for identifying and examining all potential situations, including the various factors and variables that control an investigation. The Taguchi method is used based on DOE, which incorporates experimental and theoretical approaches to refine the response's most critical parameter. Here, three factors (Test Material, Test Environment, and Applied Load) with three design levels were adopted, as illustrated in Table 2, to study the effect of control factors on Wear Rate, Temperature, and Coefficient of Friction. The degree of freedom for each control parameter is equal to one less than number of levels of that parameter. According to the rule, the minimum number of experimental runs should be one greater than the sum of degrees of freedom of all control parameters and their interactions. L27 Orthogonal array was employed for three 3-level factors, as shown in Table 3. Twenty Seven experiments based on the run order generated by the Taguchi model were carried out. The responses to the model were the Wear Rate, Temperature, and Coefficient of Friction. In the Orthogonal array, the columns assigned followed the order material, test environment, and applied load for the factors

Table 2 Control parameters and their levels

Factor	Unit	Level 1	Level 2	Level 3
Material	*	Gunmetal	LM13T10	LM13
Environment	*	TiO$_2$	MoS$_2$	Graphite
Applied load	N	50	100	150

*not available

Fig. 2 A schematic representation of the wear test assembly
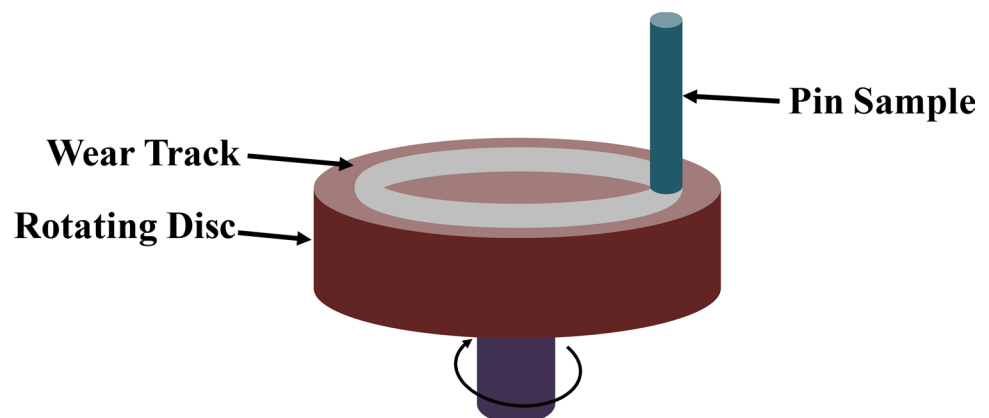
Table 3 L27 Orthogonal array of experimental layout

Experiment no.	Material	Environment	Applied load
1	1	1	1
2	1	1	1
3	1	1	1
4	1	2	2
5	1	2	2
6	1	2	2
7	1	3	3
8	1	3	3
9	1	3	3
10	2	1	2
11	2	1	2
12	2	1	2
13	2	2	3
14	2	2	3
15	2	2	3
16	2	3	1
17	2	3	1
18	2	3	1
19	3	1	3
20	3	1	3
21	3	1	3
22	3	2	1
23	3	2	1
24	3	2	1
25	3	3	2
26	3	3	2
27	3	3	2

and responses (Wear Rate, Temperature, and Coefficient of Friction) were set to the other columns. The objective of the model was to minimize the Wear Rate, Temperature, and Coefficient of Friction. S/N ratio and Mean was calculated, and results were subjected to Analysis of Variance (ANOVA).

4 Results

4.1 Microstructure

Figure 3 elicits the micrograph of the test materials. Matrix alloy comprises of dendrites of Aluminum and eutectic Si (sharp-edge plate-shaped) traces in the inter-dendritic areas. Since the eutectic structure includes both elements, the solid solubility of Si in Al is negligible. The micrograph of SiC reinforced composites delineates the uniform distribution of SiC along with the traditional characteristics of Al alloys.

The SiC particles wrapped within the primary dendrites of aluminum rather than settling down in the inter-dendritic region. Strong interfacial bonding and uniform SiC distribution in Al matrix can enhance mechanical and wear properties (explained in the following section). However, agglomeration of dispersoids leads to secure removal of dispersoids from the matrix and causing higher wear rates than the matrix alloy [27]. The Gunmetal microstructure includes primary α dendrites, intermetallic Cu–Al complex, and small iron particles.

4.2 Hardness and Density

Table 4 shows the hardness and tensile strength of the sample. The Gunmetal has significantly high hardness and tensile strength than the alloy and composite. Additionally, the inclusion of SiC particulates in the matrix alloy enhances their hardness due to a harder phase in the matrix alloy. Concerning tensile strength, the dispersion of SiC particles within the matrix lowers the tensile strength; this can result from the typical ceramic nature of SiC particles, and the bonding between Si and Al is fragile like Van der Waals bonding.

Aluminum and SiC do not react together at the processing temperature of composite materials, and therefore, there is no possibility to form interface products. There is de-cohesion at the particle–matrix interface during tensile stress, resulting in the creation of voids. In the case of coarse particles (50–100 μm) in the aluminum matrix, the likelihood of void formation is high, thus decreasing the tensile strength in composite materials [59].

4.3 Signal-to-Noise Ratio Analysis

"Smaller is better" strategy, Eq. (1) is employed to analyze Signal-to-Noise Ratio.

$$\left(\frac{S}{N}\right)_{\text{Smaller is better}} = -10\log_{10}\left(\frac{1}{n}\sum_{i=1}^{n} Y_i^2\right) \tag{1}$$

where n is the number of observations and Y_i represents the response to the wear rate.

The delta value in Table 5 indicates the effect of a factor. The delta value is the difference between the highest and lowest characteristic average for a factor. The higher the variation, the higher will be the delta value, and the greater will be the significance of that parameter on the responses. The significance of the parameter determines its rank. From the rank, it is evident that load has significant importance on Wear Rate, Temperature, and Coefficient of Friction followed by the test environment and test material.
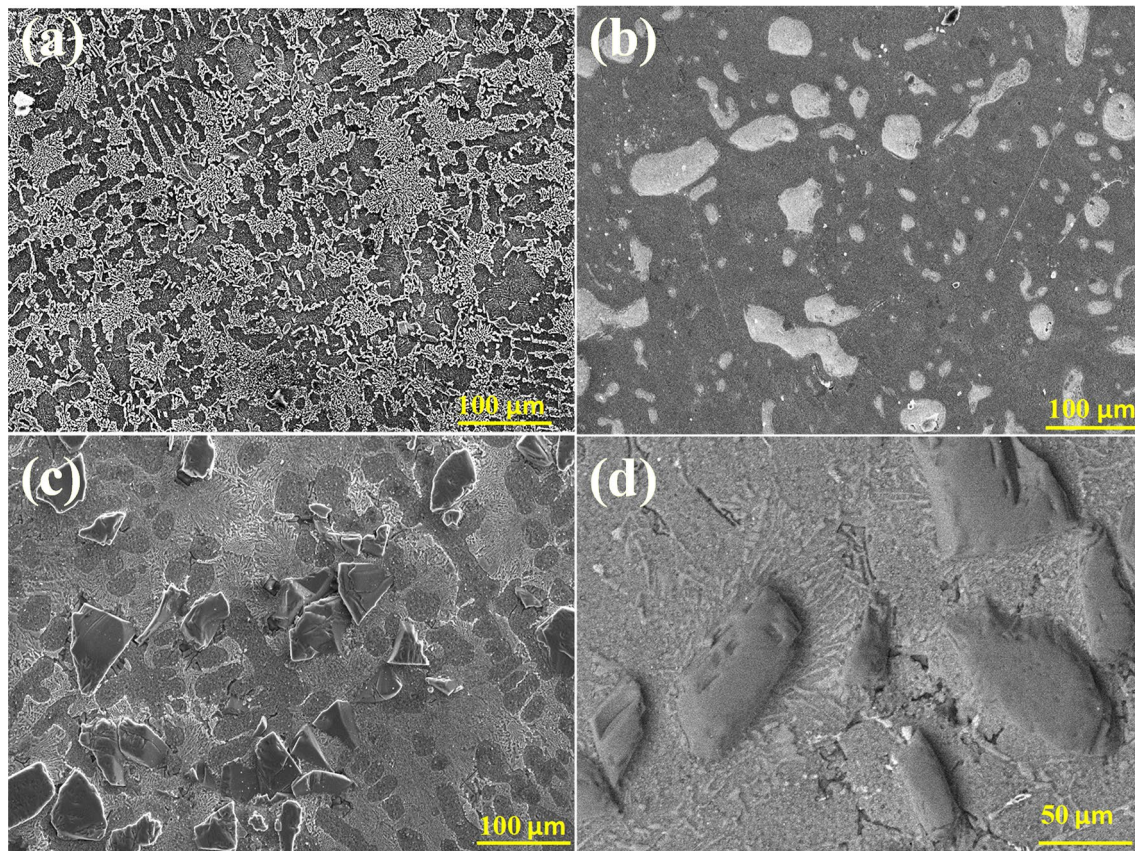
Fig. 3 Microstructural features of **a** matrix alloy, **b** gunmetal, **c**, **d** composite

Table 4 Mechanical properties of the test material

Material	Hardness (HV)	Ultimate tensile strength (MPa)
LM13	88	178
LM13S10	92	169
Gunmetal	96	212

Table 5 Response table for signal-to-noise ratio (smaller is better)

Level	Material	Environment	Applied load
1	− 27.36	− 27.36	− 26.61
2	− 27.51	− 27.36	− 27.39
3	− 27.43	− 27.58	− 28.30
Delta	0.15	0.23	1.70
Rank	3	2	1

The sliding wear rates, friction coefficient, and frictional heating for different combinations of the variables (Material, Test Environments, and Applied Load) according to Taguchi's L27 orthogonal array (OA) are given in Table 6. MINITAB software is implemented for the DOE, and after that, subsequent analysis and plots are obtained for main effects and their interactions. S/N ratio plots determine the optimum level of each control parameter. From the main effects plot, the optimum condition for the minimum wear rate was obtained as (LM13S10, MoS_2@50 N Load). Similarly, the optimum level of processing variables for Temperature (LM13, Graphite @50 N load) and COF (LM13S10, MoS_2 @ 50 N load) are obtained from the main effects plot. The graph of wear rate shows the transition to wear for different parameter levels. The wear rate is directly proportional to the applied load and inversely to the amount of reinforcement for the composite. Compared to aluminum alloy, the composite shows a lower wear rate due to hard reinforcement particles. The uniformly distributed SiC

Table 6 L27 Orthogonal array experimental layout and results

Material	Environment	Applied load	Wear	Temp	COF	SNR_wear	SNR_T	SNR_COF
LM13	TiO$_2$	50	10.79	35.41	0.096	−20.6576	−30.9825	20.38781
LM13	TiO$_2$	100	17.98	37.28	0.098	−25.0946	−31.4284	20.20507
LM13	TiO$_2$	150	29.66	39.37	0.099	−29.4443	−31.9037	20.10193
LM13	MoS$_2$	50	7.19	35.41	0.034	−17.1358	−30.9825	29.4646
LM13	MoS$_2$	100	13.89	37.13	0.044	−22.8526	−31.3945	27.05234
LM13	MoS$_2$	150	23.37	40.22	0.083	−27.3735	−32.0886	21.60798
LM13	Graphite	50	11.11	35.15	0.062	−20.9151	−30.9175	24.13817
LM13	Graphite	100	15.00	37.21	0.074	−23.5218	−31.4125	22.67031
LM13	Graphite	150	24.07	38.30	0.074	−27.6286	−31.6633	22.60754
Gunmetal	TiO$_2$	50	10.88	36.15	0.063	−20.7361	−31.1614	23.95365
Gunmetal	TiO$_2$	100	13.61	38.10	0.064	−22.6742	−31.6185	23.91721
Gunmetal	TiO$_2$	150	19.05	40.22	0.077	−25.5968	−32.0886	22.22892
Gunmetal	MoS$_2$	50	6.11	36.49	0.023	−15.7224	−31.2437	32.89225
Gunmetal	MoS$_2$	100	10.00	38.10	0.037	−20	−31.6185	28.58914
Gunmetal	MoS$_2$	150	16.67	40.45	0.059	−24.437	−32.1377	24.54379
Gunmetal	Graphite	50	8.99	35.39	0.060	−19.074	−30.9774	24.36968
Gunmetal	Graphite	100	13.48	38.25	0.074	−22.5958	−31.6533	22.65065
Gunmetal	Graphite	150	21.11	39.37	0.075	−26.4902	−31.9031	22.47564
LM13S10	TiO$_2$	50	5.56	38.04	0.030	−14.8946	−31.6057	30.59375
LM13S10	TiO$_2$	100	7.22	40.83	0.031	−17.1734	−32.2194	30.314
LM13S10	TiO$_2$	150	9.44	43.31	0.062	−19.5035	−32.7322	24.17555
LM13S10	MoS$_2$	50	4.54	36.97	0.008	−13.1318	−31.3568	42.15811
LM13S10	MoS$_2$	100	7.26	40.54	0.030	−17.2142	−32.157	30.34253
LM13S10	MoS$_2$	150	9.98	42.81	0.042	−19.9803	−32.6299	27.45951
LM13S10	Graphite	50	6.35	36.01	0.035	−16.0544	−31.1292	29.06915
LM13S10	Graphite	100	10.88	39.51	0.045	−20.7361	−31.9335	26.92289
LM13S10	Graphite	150	13.61	41.37	0.077	−22.6742	−32.3327	22.28147

Table 7 Response table for signal-to-noise ratios for wear rate (smaller is better)

Level	Material	Environment	Applied load (N)
1	−21.93	−22.19	−17.59
2	−23.85	−19.76	−21.32
3	−17.93	−21.75	−24.79
Delta	5.92	2.43	7.20
Rank	2	3	1

particles induce hardness in the composite, which resists deformation of the composite and decreases wear rate compared to unreinforced alloy.

4.4 Effects of Process Parameters on Sliding Wear

The response table (Table 7) for a signal-to-noise ratio depicts that the applied load has the highest delta value; hence the highest significance followed by the test material and test environment (Fig. 4).

The wear rate increased with applied load irrespective of the test material and lubricating environment. Applied load directly influences the wear rate, i.e., the higher the load greater the wear rate. As far as environmental impacts are concerned, much complexity exists [24, 60]. In all the test conditions, LM13 alloy delineates the maximum wear rate followed by the Gunmetal and composite. Moreover, MoS$_2$ has shown a reduced wear rate compared to graphite and TiO$_2$. It is about 50% less than others with a few exceptions.
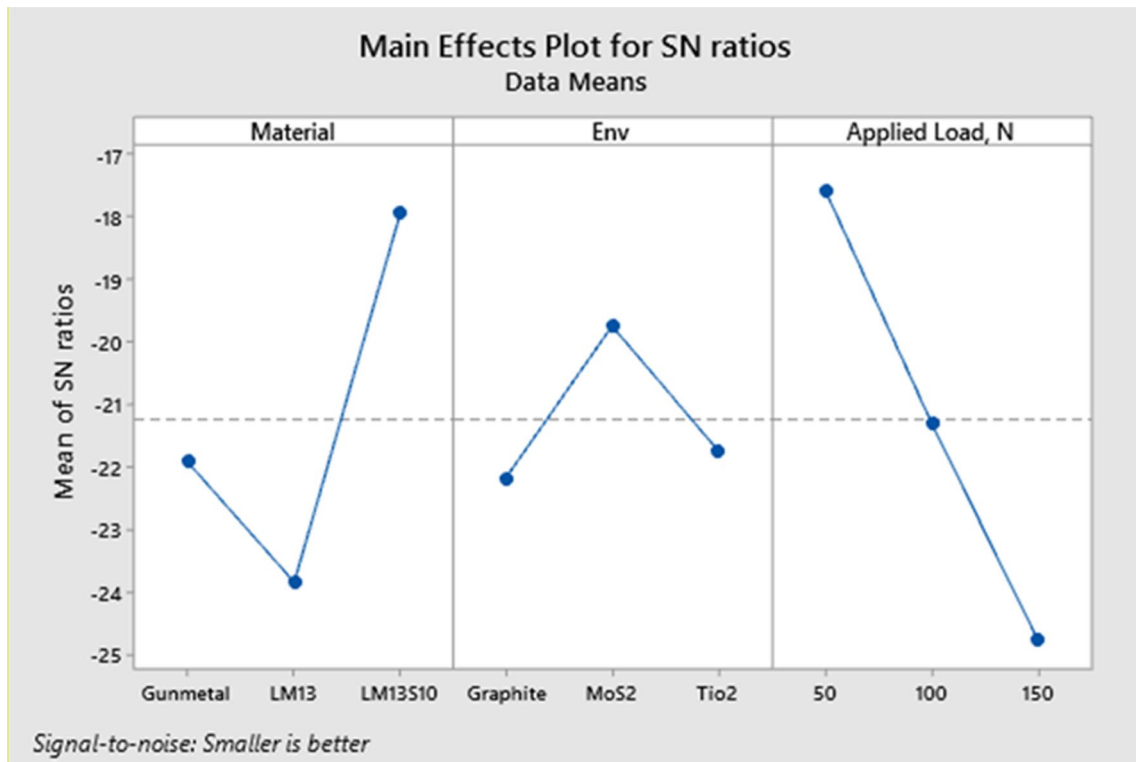
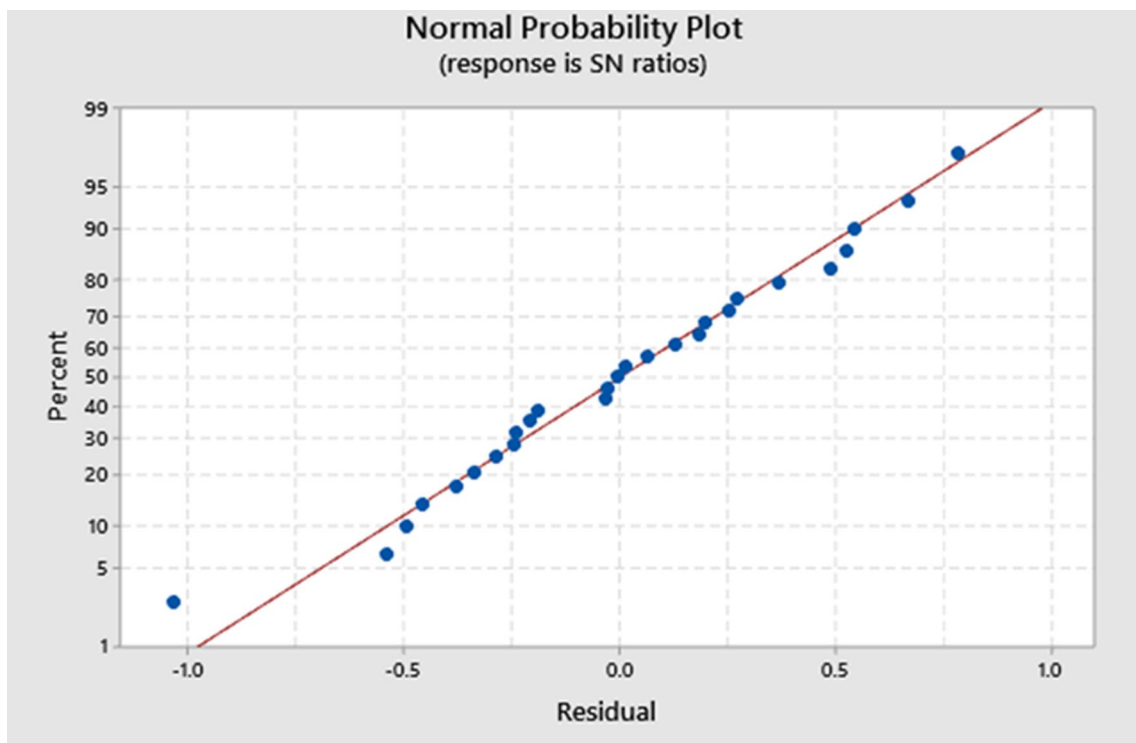**Fig. 4** Main effects plots for *S/N* ratio for wear rate

Fig. 5 Normal probability plot for residuals for wear rate

Table 8 Response table for signal-to-noise ratios for frictional heating (smaller is better)

Level	Material	Environment	Applied load (N)
1	−31.60	−31.55	−31.15
2	−31.42	−31.73	−31.72
3	−32.01	−31.75	−32.16
Delta	0.59	0.20	1.01
Rank	2	3	1

Usually, the sliding wear characteristics of material improve by the use of lubricants. The amalgamation of a solid lubricant into a liquid lubricant further improves the wear behavior by increasing the film stability. The reason being that the lubricant amalgam should not only adhere to the contacting surface but also should have enough lubricating characteristics. Normal probability plots for the residual (Fig. 5) indicate a data trend similar to the central one.

4.5 Effects of Process Parameter on Frictional heating

From the Response Table for Signal-to-Noise Ratios (Table 8), it can be seen that the applied load has the highest delta value, hence the highest significance followed by the test material and test environment (Fig. 6). The temperature increases linearly irrespective of the Load and test material. In all the test environments, maximum frictional heating is obtained in composite and minimum for the matrix alloy, while Gunmetal shows an intermediate response. The frictional heat initially increased with load; however, further increment in the load reduces the frictional heating severity.

Moreover, frictional heating of all the test materials behaved identically. The sticking tendency of the specimen material to counterface disk tends to increase the temperature at the end of tests. More severe wear conditions due to increasing applied load caused the temperature to increase rapidly. Due to the matrix alloy's excellent lubricating tendency, it exhibited the least frictional heat generation. Unlike matrix alloy, more extensive frictional heating was observed due to the abrasion caused by the fragmented dispersoid SiC particles [61]. The Gunmetal suffered maximum temperature increase irrespective of the test condition due to the fragmented cementite particles' abrasion through their entrapment between the contacting surfaces. The addition of graphite decreased frictional heating by forming a still more stable lubricating film [62]. A normal probability plot (Fig. 7) indicates that the data is normally distributed, and the residuals follow an approximately straight line.
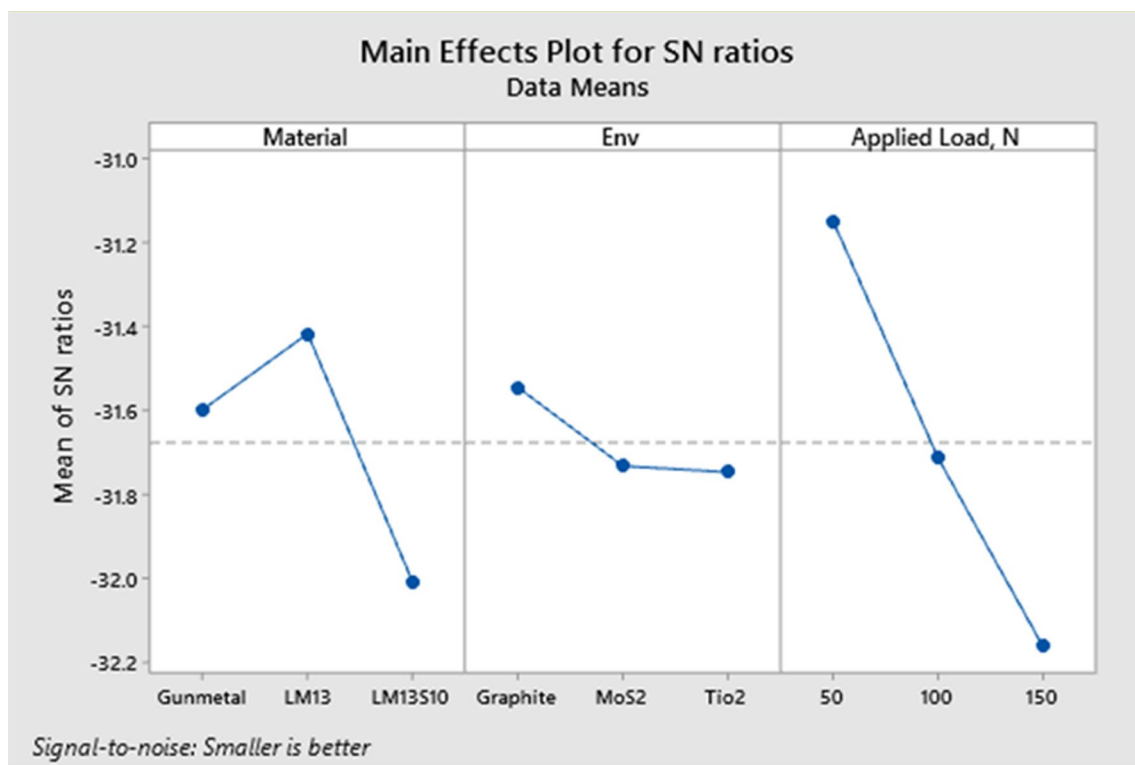
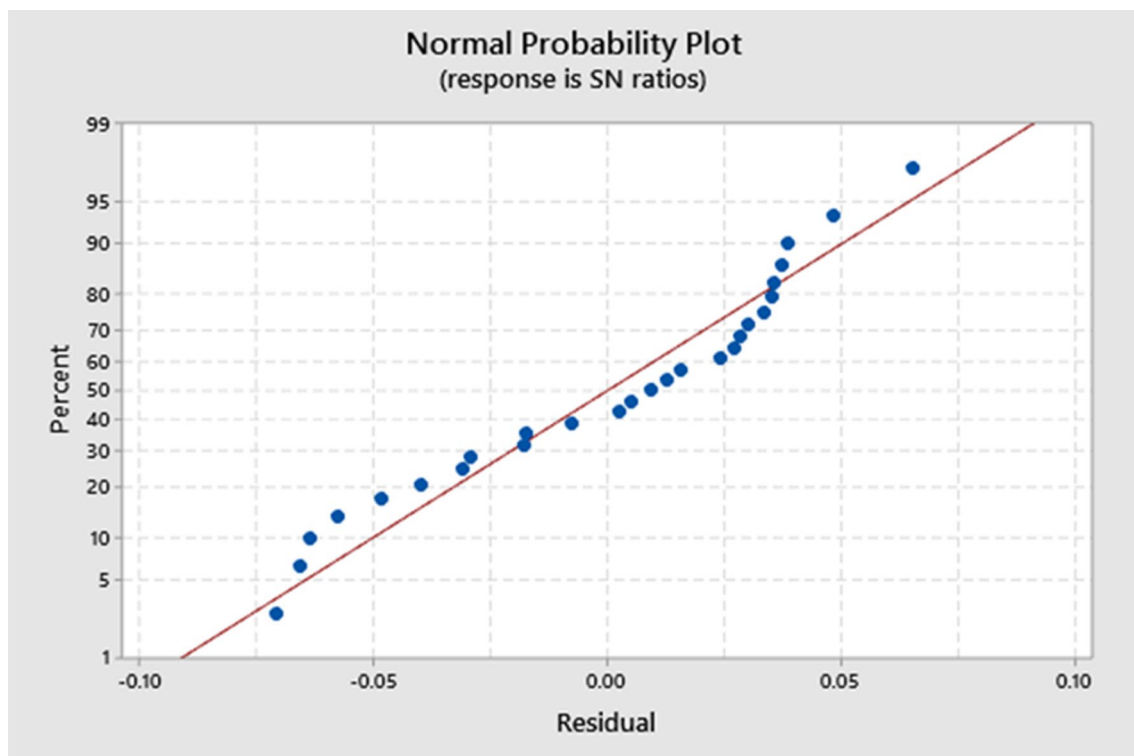**Fig. 6** Main effects plots for *S/N* ratio for frictional heating

Fig. 7 Normal probability plot for residuals for frictional heating

4.6 Effects of Process Parameter on the Coefficient of Friction

The response table (Table 9) for the signal-to-noise ratio depicts that the test material has the highest delta value; hence the highest significance, followed by the applied load and test environment (Fig. 8).The test material's friction coefficient as a function of load applied in the various lubricated test environments has been plotted. The friction coefficient continuously increased with an increasing load applied for all the test materials. The maximum friction coefficient was obtained in the LM13 alloy case, followed by

Table 9 Response table for signal-to-noise ratios (smaller is better)

Level	Material	Environment	Applied load (N)
1	25.07	24.13	28.56
2	23.14	29.35	25.85
3	29.26	23.99	23.05
Delta	6.12	5.36	5.50
Rank	1	3	2

Gunmetal and composite in all the lubricated test environments. Moreover, the MoS_2 lubricated environment delineates the minimum friction coefficient, while the maximum friction coefficient is obtained in TiO_2 lubricated environment. The lubricating and less cracking nature caused the friction coefficient of the matrix alloy to become the least. The abrasion caused by the entrapped dispersoid phase after fragmentation during wear led to the composite's higher friction coefficient than matrix alloy [38, 62, 63]. A normal probability plot (Fig. 9) indicates that the data is normally distributed.

4.7 Analysis of Variance (ANOVA)

The ANOVA was performed for the 5% significance level and 95% confidence level to identify the significance of parameters and their interactions on all the three responses (Tables 10, 11, 12, 13, 14, 15). Significance level, denoted by α is a measure of the strength of the evidence that must be present in a sample before rejecting the null hypothesis and concluding that the effect is statistically significant. P-value, the probability that measures the evidence against
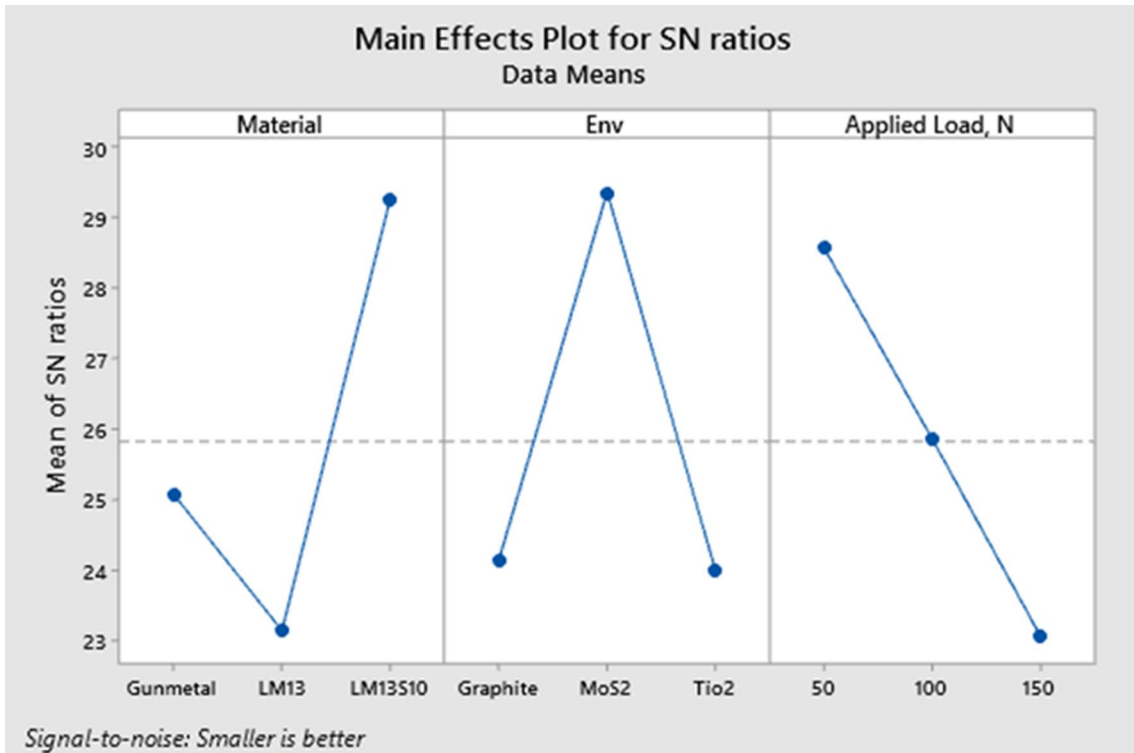
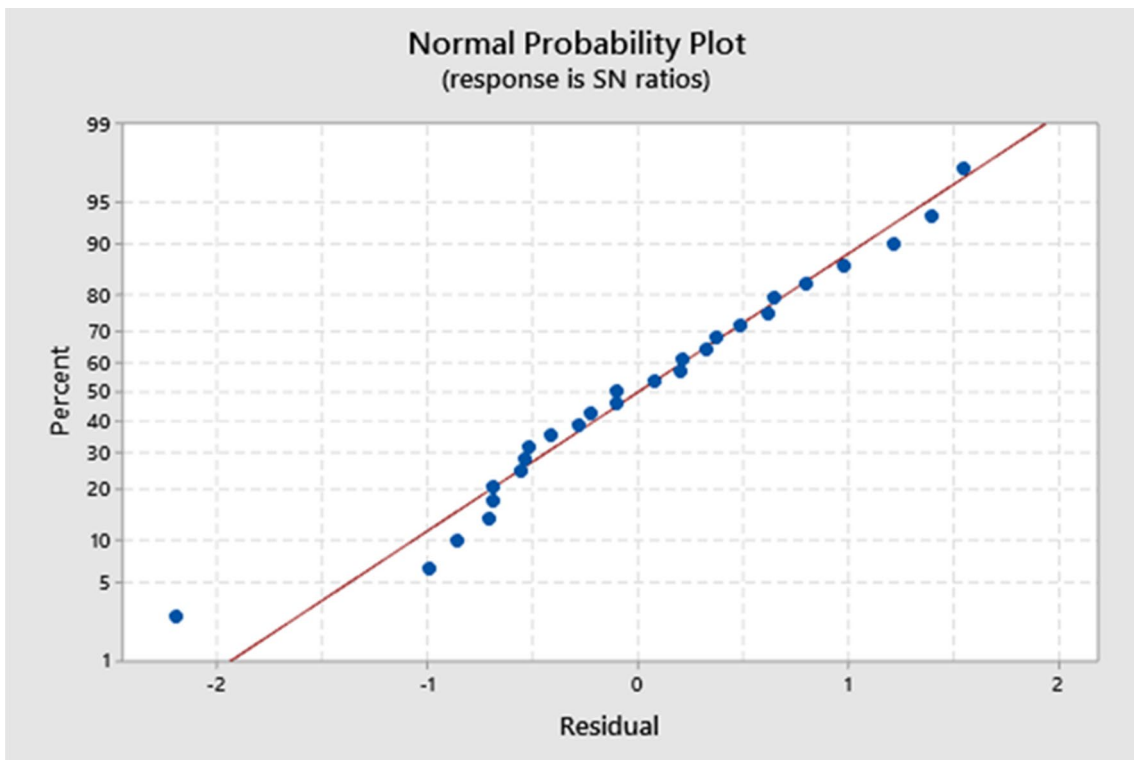**Fig. 8** Main effects plots for *S/N* ratio for the friction coefficient

Fig. 9 Normal probability plot of residuals for friction coefficient

Table 10 Analysis of variance for wear rates

Source	Degree of freedom	Sum of squares	Adjusted sum of square	Adjusted mean Square	F	P	% Contribution
Material	2	164.051	164.051	82.025	142.77	0.000	35.99
Environment	2	30.142	30.142	15.071	26.23	0.000	6.61
Applied load (N)	2	233.423	233.423	116.712	203.15	0.000	51.21
Material × environment	4	12.490	12.490	3.122	5.43	0.021	2.74
Material × applied load (N)	4	5.911	5.911	1.478	2.57	0.119	1.30
Environment × applied load (N)	4	5.229	5.229	1.307	2.28	0.150	1.15
Residual error	8	4.596	4.596	0.575			1.01
Total	26	455.841					

Table 11 Model summary for wear rate

S	R^2 (%)	Adjusted R^2 (%)
0.7580	98.99	96.72

Table 13 Model summary for temperature

S	R^2(%)	Adjusted R^2 (%)
0.0706	99.41	98.09

the null hypothesis, if smaller than the significance level (as observed in the present study), advocates the rejection of the null hypothesis; otherwise, it accepts the null hypothesis. Each parameter's percentage significance is found out and indicated in the last column of Tables 10, 12, and 14 for wear rate, frictional heating, and friction coefficient, respectively. From Table 10, it is observed that applied load has higher significance (51.21%) on wear rate, followed by test material (35.99%), and test environment (6.61%). Moreover, Table 12 delineates that the load has higher significance (68.22%) on wear rate, followed by test material (24.28%), and test environment (3.36%).Furthermore, it has been observed that the test material has higher significance (28.79%) on wear rate,

followed by test environment (27.41%) and load (22.28%), as depicted in Table 14.

4.8 Confirmation Experiments

After identifying the most influential parameters, the final phase is to verify the responses by conducting the confirmation experiments. The LM13S10 composite under MoS_2 lubrication at 50 N load is an optimal parameter combination during the wear test. Therefore, the condition of the optimal parameter combination was treated as a confirmation test. The confirmation test result gives the wear rate, temperature, and friction coefficient similar to those shown in Table 6.

Table 12 Analysis of variance for temperature

Source	Degree of freedom	Sum of squares	Adjusted sum of square	Adjusted mean square	F	P	% Contribution
Material	2	1.65294	1.65294	0.82647	165.67	0.000	24.28
Environment	2	0.22845	0.22845	0.11422	22.90	0.000	3.36
Applied load (N)	2	4.64374	4.64374	2.32187	465.43	0.000	68.22
Material × environment	4	0.08011	0.08011	0.02003	4.01	0.045	1.18
Material × applied load (N)	4	0.10206	0.10206	0.02551	5.11	0.024	1.50
Environment × applied load (N)	4	0.05949	0.05949	0.01487	2.98	0.088	0.87
Residual error	8	0.03991	0.03991	0.00499			0.59
Total	26	6.80669					

Table 14 Analysis of variance for the coefficient of friction

Source	Degree of freedom	Sum of squares	Adjusted sum of square	Adjusted mean square	F	P	%Contribution
Material	2	176.19	176.19	88.096	39.04	0.000	28.79
Environment	2	167.78	167.78	83.889	37.17	0.000	27.41
Applied Load (N)	2	136.38	136.38	68.192	30.22	0.000	22.28
Material × environment	4	23.43	23.43	5.859	2.60	0.117	3.83
Material × applied load (N)	4	33.01	33.01	8.252	3.66	0.056	5.39
Environment × applied load (N)	4	57.20	57.20	14.299	6.34	0.013	9.35
Residual error	8	18.05	18.05	2.257			2.95
Total	26	612.05					

Table 15 Model summary for the coefficient of friction

S	R^2 (%)	Adjusted R^2 (%)
1.5022	97.05	90.41

4.9 Worn Surface Analysis

The scanning electron microscope (SEM) analysis is used to understand the test specimens' worn surface mechanisms. Figure 10 delineates the worn surface of the SiC reinforced composite at 150 N for MoS_2, TiO_2, and Graphite lubricated environment. In the MoS_2 lubricated environment, the material removal rate observed was minimal due to layers' delamination. In contrast, in the TiO_2 environment, the abraded burrs formed during the wear cause three-body abrasions. However, in a lubricated graphite environment, the presence of suspended graphite particles in the oil lubricant proved to be still more effective towards forming a stable lubricating film on the contacting surfaces. Formation of dark patches on the wear surfaces and orientation/flow of graphite present within the sample material in sliding direction.

5 Conclusions

The liquid metallurgy route was adopted to synthesize SiC reinforced aluminum matrix composite. The effects of applied load and adding solid lubricants (MoS_2, TiO_2, and graphite) to the oil during the developed composite's sliding behavior have been experimentally investigated using a pin-on-disk machine and compared with the matrix alloy as well as conventionally used Gunmetal. The ANOVA analysis based on the Taguchi method's response table was used to optimize the test parameters. Based on the results of the present study, the following conclusions are drawn:

- MoS_2 shows a 20–35% reduction in wear rate than other lubricants at all the applied loads.
- Wear rate, coefficient of friction, and frictional heating all increased with an increase in the applied load.
- MoS_2 and graphite show the lowest temperature profiles owing to outstanding lubricity and surface adhesion.

The results' anticipation establishes that SiC reinforced aluminum alloys are more favorable than the traditional Gunmetal under lubricated environments.
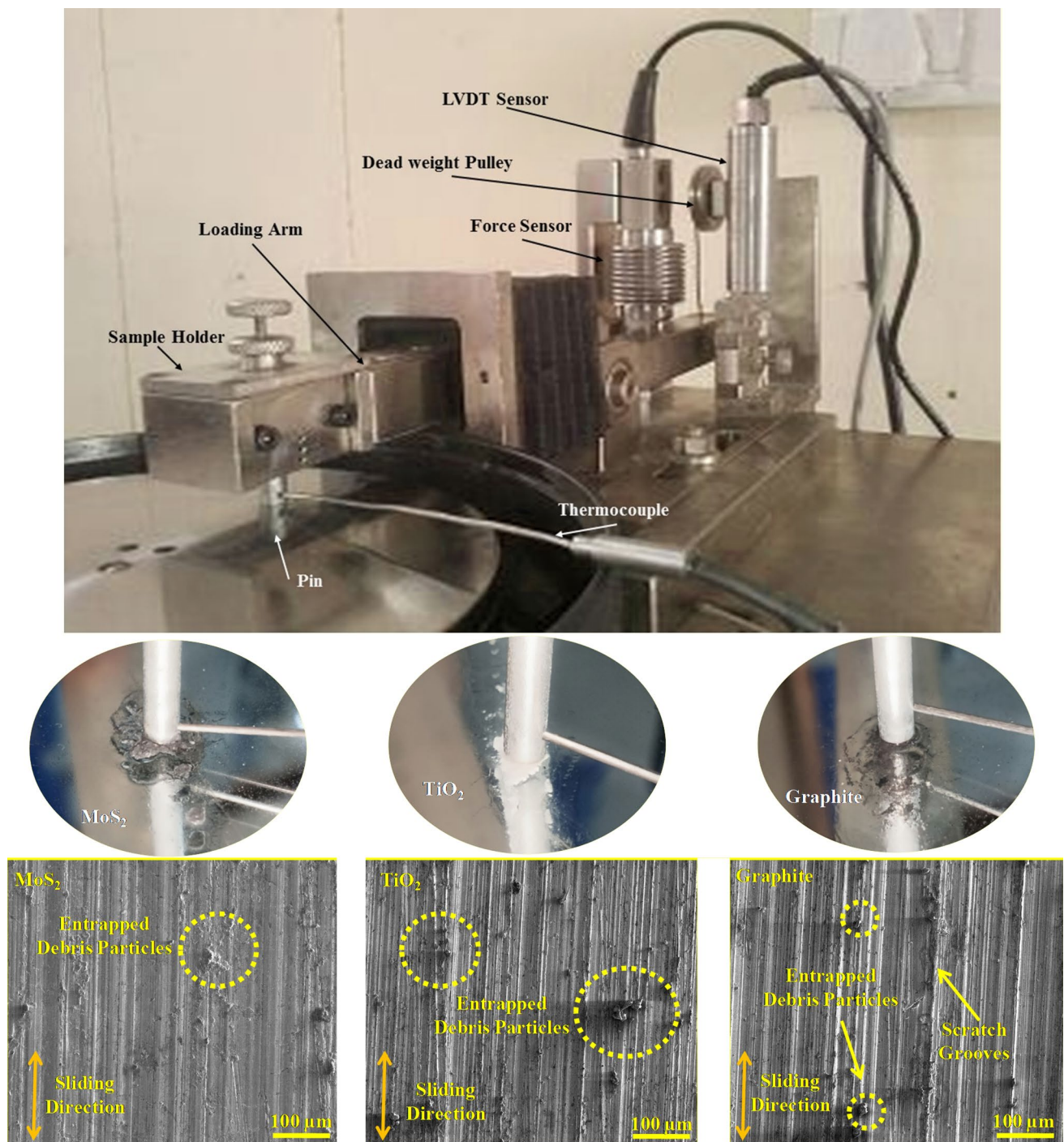
Fig. 10 Schematic of the wear test with worn out surface images

References

1. Khan MM, Dixit G (2018) Abrasive Wear characteristics of silicon carbide particle reinforced zinc based composite. Silicon 10(4):1315–1327

2. Saravanan G, Shanmugasundaram K, Prakash M, Velayudham A (2015) Tribological behaviour of hybrid (Al356+ SiC+ Gr) metal matrix composites. Appl Mech Mater 766:269–275

3. Khan MM, Dixit G (2017) Comparative study on erosive wear response of SiC reinforced and fly ash reinforced aluminium based metal matrix composite. Mater Today Proc 4(9):10093–10098

4. AZom (2020) https://www.azom.com/article.aspx?ArticleID=6588 Google Scholar. https://scholar.google.com/scholar?hl=en&as_sdt=0%2C5&q=AZom.+https%3A%2F%2Fwww.azom.com%2Farticle.aspx%3FArticleID%3D6588&btnG=. Accessed 8 Oct 2020

5. Cheneke S, Benny Karunakar D (2019) The effect of solution treatment on aging behavior and mechanical properties of AA2024-TiB2 composite synthesized by semi-solid casting. SN Appl. Sci. 1(11):1501. https://doi.org/10.1007/s42452-019-1531-z

6. Xiu Z et al. (2020) "Microstructure and tensile properties of Si3N4p/2024Al composite fabricated by pressure infiltration method. Elsevier, New York. https://www.sciencedirect.com/science/article/pii/S0261306911001567. Accessed 09 Oct 2020

7. Kok M (2005) Production and mechanical properties of Al_2O_3 particle-reinforced 2024 aluminium alloy composites. Journal of materials processing technology and undefined 2005, Elsevier, New York https://www.sciencedirect.com/science/article/pii/S0924013604009471. Accessed 09 Oct 2020

8. Kumar KA, Natarajan S, Duraiselvam M, Ramachandra S (2019) Synthesis, characterization and mechanical behavior of Al 3003: TiO_2 surface composites through friction stir processing. Mater Manuf Process 34(2):183–191. https://doi.org/10.1080/10426914.2018.1544711

9. Ahmadi E, Ranjkesh M, Mansoori E et al (2017) Microstructure and mechanical properties of Al/ZrC/TiC hybrid nanocomposite filler metals of tungsten inert gas welding fabricated by accumulative roll. Journal of manufacturing process and undefined 2017, Elsevier, New York. https://www.sciencedirect.com/science/article/pii/S1526612517300415. Accessed 08 Oct 2020

10. Samal P, Vundavilli PR, Meher A, Mahapatra MM (2019) Fabrication and mechanical properties of titanium carbide reinforced aluminium composites. Mater Today 18:2649–2655. https://doi.org/10.1016/j.matpr.2019.07.125

11. Mohan A, Gautam G, Kumar N, Mohan S, Gautam RKC (2016) Synthesis and tribological properties of AA5052-base in situ composites. Compos Interfaces 23(6):503–518. https://doi.org/10.1080/09276440.2016.1155386

12. Bauri R, Yadav D, Kumar C, Balaji B (2015) Tungsten particle reinforced Al 5083 composite with high strength and ductility. Material Science and Engineering, and undefined 2015, Elsevier, New York. https://www.sciencedirect.com/science/article/pii/S0921509314012246. Accessed 08 Oct 2020

13. Prashantha Kumar HG, Anthony Xavior M (2017) Effect of graphene addition and tribological performance of Al 6061/graphene flake composite. Tribol 11(2):88–97. https://doi.org/10.1080/17515831.2017.1329920

14. Dinaharan I, Murugan N (2012) Optimization of friction stir welding process to maximize tensile strength of AA6061/ZrB2 in-situ composite butt joints. Met Mater Int 18(1):135–142. https://doi.org/10.1007/s12540-012-0016-z

15. Umanath K, Palanikumar K, Selvamani S (2013) Analysis of dry sliding wear behaviour of Al6061/SiC/Al_2O_3 hybrid metal matrix composites. Composites Part B: Engineering and undefined 2013, Elsevier, New York. https://www.sciencedirect.com/science/article/pii/S1359836813001996. Accessed 09 Oct 2020

16. Kumar G, Rao C, Selvaraj N (2012) Studies on mechanical and dry sliding wear of Al6061–SiC composites. Composites Part B: Engineering, and undefined 2012. Elsevier, New York. https://www.sciencedirect.com/science/article/pii/S1359836811003805. Accessed 09 Oct2020

17. Kalaiselvan K, Murugan N, Parameshwaran S (2011) Production and characterization of AA6061-B4C stir cast composite. Materials and Design, and undefined 2011. Elsevier, New York. https://www.sciencedirect.com/science/article/pii/S0261306911001750. Accessed 09 Oct 2020

18. Samal P, Mandava RK, Vundavilli PR (2020) Dry sliding wear behavior of Al 6082 metal matrix composites reinforced with red mud particles. SN Appl Sci 2(2):1–11. https://doi.org/10.1007/s42452-020-2136-2

19. Rejil CM, Dinaharan I, Vijay SJ, Murugan N (2012) Microstructure and sliding wear behavior of AA6360/(TiC+B 4C) hybrid surface composite layer synthesized by friction stir processing on aluminum substrate. Mater Sci Eng A 552:336–344. https://doi.org/10.1016/j.msea.2012.05.049

20. Al-Salihi HA, Mahmood AA, Alalkawi HJ (2019) Mechanical and wear behavior of AA7075 aluminum matrix composites reinforced by Al_2O_3 nanoparticles. Nanocomposites 5(3):67–73. https://doi.org/10.1080/20550324.2019.1637576

21. Kumar A, Pal K, Mula S (2017) Simultaneous improvement of mechanical strength, ductility and corrosion resistance of stir cast Al7075-2% SiC micro- and nanocomposites by friction stir processing. J Manuf Process 30:1–13. https://doi.org/10.1016/j.jmapro.2017.09.005

22. Hu Q, Zhao H, Li F (2016) Effects of manufacturing processes on microstructure and properties of Al/A356–B4C composites. Mater Manuf Process 31(10):1292–1300. https://doi.org/10.1080/10426914.2016.1151049

23. Mazahery A, Shabani MO, Salahi E, Rahimipour MR, Tofigh AA, Razavi M (2012) Hardness and tensile strength study on Al356-B 4C composites. Mater Sci Technol 28(5):634–638. https://doi.org/10.1179/1743284710Y.0000000010

24. Dixit G, Khan MM (2014) Sliding wear response of an aluminium metal matrix composite: effect of solid lubricant particle size. Jordan J Mech Ind Eng 8:6

25. Mohanavel V (2019) Synthesis and evaluation on mechanical properties of LM4/AlN alloy based composites. Energy Sources A. https://doi.org/10.1080/15567036.2019.1647313

26. Chelladurai SJS, Arthanari R, Nithyanandam N, Rajendran K, Radhakrishnan KK (2018) Investigation of mechanical properties and dry sliding wear behaviour of squeeze cast LM6 aluminium alloy reinforced with copper coated short steel fibers. Trans Indian Inst Met 71(4):813–822. https://doi.org/10.1007/s12666-017-1258-8

27. Khan MM, Dixit G (2019) Evaluation of microstructure, mechanical, thermal and erosive wear behavior of aluminum-based composites. Silicon 12(1):1–12. https://doi.org/10.1007/s12633-019-00099-4

28. Prasad SV, Asthana R (2004) Aluminum metal-matrix composites for automotive applications: tribological considerations. Tribol Lett 17(3):445–453. https://doi.org/10.1023/B:TRIL.0000044492.91991.f3

29. Srivastava VC, Ojha SN (2005) Microstructure and electrical conductivity of Al-SiC p composites produced by spray forming process. Bull Mater Sci. https://doi.org/10.1007/BF02704231.pdf

30. Khan M (2017) Erosive wear response of SiCp reinforced aluminium based metal matrix composite: effects of test environments. Artic J Mech Eng Sci. https://doi.org/10.15282/jmes.11.1.2017.1.0222

31. Bansal S, Saini JS (2015) Mechanical and wear properties of SiC/graphite reinforced Al359 alloy-based metal matrix composite. Def Sci J 65(4):330–338. https://doi.org/10.14429/dsj.65.8676

32. Kamrani S, Riedel R, Seyed Reihani SM, Kleebe HJ (2010) Effect of reinforcement volume fraction on the mechanical properties of Alg-SiC nanocomposites produced by mechanical alloying

and consolidation. J Compos Mater 44(3):313–326. https://doi.org/10.1177/0021998309347570

33. Sujith SV, Mahapatra MM, Mulik RS (2020) Microstructural characterization and experimental investigations into two body abrasive wear behavior of Al-7079/TiC in-situ metal matrix composites. Proc Inst Mech Eng 234(4):588–607. https://doi.org/10.1177/1350650119883559

34. Huang G, Wu J, Hou W, Shen Y, Gao J (2019) Producing of Al–WC surface composite by additive friction stir processing. Mater Manuf Process 34(2):147–158. https://doi.org/10.1080/10426914.2018.1532590

35. Mazahery A, Ostadshabani M (2011) Investigation on mechanical properties of nano-Al₂O₃-reinforced aluminum matrix composites. J Compos Mater 45(24):2579–2586. https://doi.org/10.1177/0021998311401111

36. Sadeghi B, Shamanian M, Ashrafizadeh F, Cavaliere P, Rizzo A (2018) Friction stir processing of spark plasma sintered aluminum matrix composites with bimodal micro- and nano-sized reinforcing Al₂O₃ particles. J Manuf Process 32:412–424. https://doi.org/10.1016/j.jmapro.2018.03.013

37. Rahimian M, Ehsani N et al (2009) The effect of particle size, sintering temperature and sintering time on the properties of Al–Al₂O₃ composites, made by powder metallurgy. Journal of Materials Processing Technology, and undefined 2009. Elsevier, New York. https://www.sciencedirect.com/science/article/pii/S0924013609001393. Accessed 09 Oct 2020

38. Zhang Q, Gu J, Wei S, Qi M (2019) Differences in dry sliding wear behavior between Al–12Si–CuNiMg alloy and its composite reinforced with Al₂O₃ fibers. Materials 12(11):1749

39. Parveen A, Chauhan NR, Suhaib M (2019) Mechanical and tribological behaviour of Al-ZrO₂ composites: a review. In: Lecture notes in mechanical engineering. Pleiades Publishing, Moscow, pp 217–229

40. Ramachandra M et al (2016) Evaluation of Corrosion Property of Aluminium-Zirconium Dioxide (AlZrO₂) Nanocomposites. International Journal of Materials and Metallurgical Engineering, and undefined 2016, publications.waset.org. http://publications.waset.org/10005637/evaluation-of-corrosion-property-of-aluminium-zirconium-dioxide-alzro2-nanocomposites. Accessed 09 Oct 2020

41. He N, Zhang J, Jin Y, Han F, Zhang X, Chen G (2019) Preparation, microstructures and mechanical properties of in-situ TiB2/Al composites by mechanical stirring and subsequent ultrasonic treatment. Mater Res Express 6(11):116553. https://doi.org/10.1088/2053-1591/ab471f

42. Ko SY et al (2013) Manufacture of CNTs-Al powder precursors for casting of CNTs-Al matrix composites. Mater Sci Forum 765:353–357. https://doi.org/10.4028/www.scientific.net/MSF.765.353

43. Samal P, Raj R, Mandava RK, Vundavilli PR (2020) Effect of red mud on mechanical and microstructural characteristics of aluminum matrix composites. Lect Notes Mech Eng. https://doi.org/10.1007/978-981-15-1307-7_8

44. Omrani E, Moghadam AD, Menezes PL, Rohatgi PK (2016) Influences of graphite reinforcement on the tribological properties of self-lubricating aluminum matrix composites for green tribology, sustainability, and energy efficiency: a review. Int J Adv Manuf Technol 83(1–4):325–346. https://doi.org/10.1007/s00170-015-7528-x

45. Bodunrin MO, Alaneme KK, Chown LH (2015) Aluminium matrix hybrid composites: a review of reinforcement philosophies; mechanical, corrosion and tribological characteristics. J Mater Res Technol 4(4):434–445. https://doi.org/10.1016/j.jmrt.2015.05.003

46. Amirkhanlou S, Rezaei M, Niroumand B (2011) High-strength and highly-uniform composites produced by compocasting and cold rolling processes. Materials and Design, and undefined 2011, Elsevier, New York. https://www.sciencedirect.com/science/article/pii/S0261306910006722. Accessed 09 Oct 2020

47. Srinivasarao B, Suryanarayana C et al (2009) Microstructure and mechanical properties of Al–Zr nanocomposite materials. Materials Science and Engineering A, and undefined 2009, Elsevier, New York. https://www.sciencedirect.com/science/article/pii/S0921509309005206. Accessed 09 Oct 2020

48. Ravindran P, Manisekar K, Narayanasamy R, Narayanasamy P (2013) Tribological behaviour of powder metallurgy-processed aluminium hybrid composites with the addition of graphite solid lubricant. Ceram Int 39(2):1169–1182

49. Li B, Chao C (1996) Mechanical properties and 95 aging characteristics of zircon-reinforced Zn-4AI-3Cu alloy. Metallurgical and Materials Transactions A, and undefined 1996, Springer, New York. https://link.springer.com/content/pdf/. Accessed 10 Oct 2020

50. Sahin Y (1998) Wear behaviour of planar-random fibre-reinforced metal matrix composites. Wear and undefined 1998, Elsevier, New York. https://www.sciencedirect.com/science/article/pii/S0043164898003159Accessed 10 Oct 2020

51. Zhu H, Liu S (1993) Mechanical properties of squeeze-cast zinc alloy matrix composites containing α-alumina fibres. Composites, and undefined 1993, Elsevier, New York. https://www.sciencedirect.com/science/article/pii/0010436193902513. Accessed 10 Oct 2020

52. Yu S, He Z, Chen K (1996) Dry sliding friction and wear behaviour of short fibre reinforced zinc-based alloy composites. Wear, and undefined 1996, Elsevier, New York. https://www.sciencedirect.com/science/article/pii/0043164896069402. Accessed 10 Oct 2020

53. Genel K, Kurnaz S, Durman M (2003) Modeling of tribological properties of alumina fiber reinforced zinc–aluminum composites using artificial neural network. Material Science and Engineering A, and undefined 2003, Elsevier, New York. https://www.sciencedirect.com/science/article/pii/S0921509303006233. Accessed 10Oct 2020

54. Prasad B (2003) Influence of some material and experimental parameters on the sliding wear behaviour of a zinc-based alloy, its composite and a bronze. Wear and undefined 2003, Elsevier, New York. https://www.sciencedirect.com/science/article/pii/S0043164802003034. Accessed 10 Oct 2020

55. Prasad BK (2007) Investigation into sliding wear performance of zinc-based alloy reinforced with SiC particles in dry and lubricated conditions. Wear 262(3–4):262–273

56. Vadiraj A, Kamaraj M, Sreenivasan VS (2011) Wear and friction behavior of alloyed gray cast iron with solid lubricants under boundary lubrication. Tribol Int 44(10):1168–1173

57. Fisher R (1925) Statistical methods for research workers Oliver and Boyd, London. In: Reprinted in statistical methods, experimental design and scientific inference. Wiley, Hoboken

58. " ASTM (2010) A standard-for wear testing with a pin-on-disk apparatus and undefined 2010, G99-5, 2010

59. Khan MM, Dixit G (2017) Effects of test parameters and SiCp reinforcement on the slurry erosive wear response of Al-Si alloy. Mater Today Proc 4(2):3141–3149

60. De Pellegrin DV, Torrance AA, Haran E (2009) Wear mechanisms and scale effects in two-body abrasion. Wear 266(1–2):13–20

61. Prasad BK, Modi OP, Khaira HK (2004) High-stress abrasive wear behaviour of a zinc-based alloy and its composite compared

with a cast iron under varying track radius and load conditions. Mater Sci Eng A 381(1–2):343–354

62. Prasad B (2007) Investigation into sliding wear performance of zinc-based alloy reinforced with SiC particles in dry and lubricated conditions. Wear and undefined 2007, Elsevier, New York. https://www.sciencedirect.com/science/article/pii/S0043164800 600202X. Accessed 09 Oct 2020

63. Pauschitz A, Roy M, Franek F (2008) Mechanisms of sliding wear of metals and alloys at elevated temperatures. Tribol Int 41(7):584–602

Publisher's Note Springer Nature remains neutral with regard to jurisdictional claims in published maps and institutional affiliations.